








# High-Speed Electric Drives: A Step Towards System Design

FILIPPO SAVI <sup>1</sup> (Student Member, IEEE), DAVIDE BARATER <sup>2</sup> (Member, IEEE),  
MAURO DI NARDO <sup>3</sup> (Member, IEEE), MICHELE DEGANO <sup>1,3</sup> (Member, IEEE),  
CHRIS GERADA <sup>1,3</sup> (Senior Member, IEEE), PAT WHEELER <sup>1,3</sup> (Senior Member, IEEE),  
AND GIAMPAOLO BUTICCHI <sup>1,3</sup> (Senior Member, IEEE)

(Invited Paper)

<sup>1</sup>Zhejiang Key Laboratory on the More Electric Aircraft Technologies, University of Nottingham Ningbo China, Ningbo 315100, China

<sup>2</sup>Department of Engineering Enzo Ferrari, University of Modena and Reggio Emilia, 41125 Modena, Italy

<sup>3</sup>The University of Nottingham, Nottingham NG72RD, U.K.

CORRESPONDING AUTHOR: G. BUTICCHI (e-mail: buticchi@ieee.org)

This work was supported by the Ningbo Science & Technology Bureau under Grants 2018B10001, 2018B10002, and 2018B10082.

---

**ABSTRACT** Electric drives applications have been worldwide adopted for the transportation electrification. An electric drive system is constituted by two main components: the power electronics converter and the electrical machine. Traditionally the design workflow consisted in the separate realization of these two parts, by different teams or even organizations. This requires strong assumptions regarding operating conditions and may lead to actual performance at system level far from the one expected. In this article, a unified design methodology of the two sub-systems is presented considering the true operating conditions, allowing a more accurate assessment of power losses at system level and identifying the influence of the converter design choices on the electric machine performance. As a case study, this article presents a comparative analysis among three different converter topologies designed to drive a 8.5 kW–120 krpm surface PMSM. The study aims at comparing the considered systems in terms of overall efficiency, losses distribution and system complexity. At first converters are simulated in Matlab-Simulink to estimate the losses and the current waveforms, that are then used in the Finite Element model of the electrical machine to estimate the loss components in a real scenario. The models developed are then validated by means of experimental measurements. This article highlights the new understanding that can be gained by considering the interactions between sub-systems, allowing a more conscious choice of the converter topology to achieve optimal overall performance.

**INDEX TERMS** Electric machine, power electronics, pulsewidth modulated power converter.

---

## I. INTRODUCTION

The design of electrical drive system dates back to several decades ago. The development of the technology and of the design methodology allowed for an ever-increasing level of performance for the electrical machine, the power electronics and the control system. Recently, the push for a more sustainable transportation has fueled the research on electrification across different sectors, such as automotive, marine and aerospace [1]. For example, in aircraft electrification systems, the integration of the electrical generation directly inside the

main jet engine has been a focus of several studies, aiming to reduce system complexity and boost both reliability and efficiency [2]. This concept, named *More Electric Engine (MEE)*, proposes the use of high speed electrical machines, in order to eliminate or reduce the need for a complex gearbox system used to drive the electrical machine at a fixed number of revolution per minute, irrespective of main shaft speed. In modern engines, the generator can be connected to either the high or low pressure shaft; the first leads to better system performance, while facing higher cost and complexity on the

machine due to the harsh operating environment. Apart from the aviation sector, numerous industrial application benefit from higher speed electrical machines, as shown in [3]–[5]. Applications like turbochargers, micro-turbines, spindle motors, turbo molecular pumps, oil and gas compressor and many others can attain higher efficiency by direct coupling of machine and load avoiding geared, belt or turbine driven transmission arrangements [6]. The drawback of an increased speed is a higher complexity in the design phase due to several mechanical, thermal, electronics and control challenges that need to be addressed [7]. The electrical machine will present additional losses due to the higher current frequencies, both in laminations and conductors, also a higher rotor rigidity is needed to insure structural integrity. From the power electronics and control perspective the synthesis of higher frequency currents with low harmonic content whilst maintaining high power density is the main challenge. The adoption of wide bandgap materials, such as silicon carbide (SiC) or Gallium Nitride (GaN), allows an increase in switching frequency and/or lower switching losses compared to standard silicon (Si) devices, helping to overcome these problems. In particular, this grants better controllability thanks to the higher ratio between switching and fundamental frequency and reduces the need for bulky output filters. However, wide bandgap devices may also result in increased electromagnetic interference EMI. Both differential and common mode components of the converter output voltage can contribute to the problem. Radiated emissions are due to the fast voltage and high current transients, whereas common mode variations are responsible for circulating currents and conducted emissions. This may negatively affect the surrounding low-power electronics and leads to premature bearing failure and increased stress on the motor windings insulation. These issues, along with mitigation strategies, are widely covered in a number of works and their extensive discussion is beyond the scope of this paper [8]–[10]. One aspect in the design of a high speed drive system that must not be overlooked is the effects that the converter topology choice has upon the performance of the whole system. The independent evaluation of converter and electrical machine [11], [12], does not always allow a correct prediction of the overall system efficiency. In fact, on one hand, machine efficiency and power factor need to be maximized in order to reduce the converter rating as much as possible, for better power density and lower cost. On the other hand, converter output power quality and topology affect the machine efficiency [13]. The selection of the most suitable electrical machine and/or converter topology for a high speed for a given high speed application, is already been studied [14]. This study, as opposed to others, aims to evaluate the effects of converter architecture choice on the electrical machine performance, usually neglected in the analysis. This paper proposes a paradigm change. While the traditional design workflow, adopted until now, involves separate design and optimization of the different system components (often performed by different engineers) to be then integrated into the final system, with the proposed new design methodology

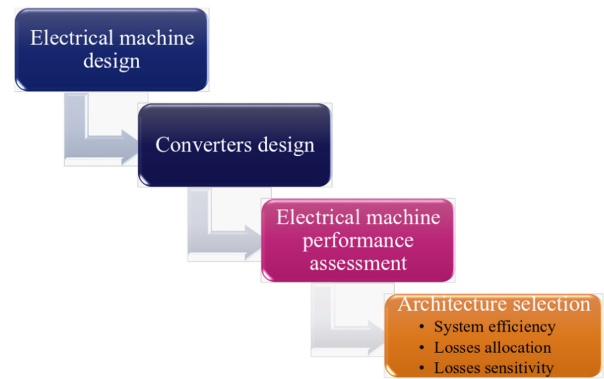


FIGURE 1. Simulation process overview.

instead, a comprehensive system level analysis is carried out. The influence of the converter choice on the overall system performance, in terms of system efficiency, losses allocation and losses sensitivity to design parameters is considered, as outlined in Fig. 1. This solution aims to achieve a true system level optimum, that was usually not possible with previous techniques. The system architecture selection is then finalized considering the system efficiency, the losses allocation and the losses sensitivity with the change of the most influential parameters. In the two next sections an overview of the electrical machines and converter structures commonly adopted for high speed applications is presented. Section IV describes the simulation environment and the losses calculation methods for both converters and electrical machine. Section V illustrates the simulation results of converters and electrical machine in terms of losses in the torque-speed plane. Section VI compares the different architectures in terms of system losses, their allocation and their sensitivity with respect to the parameter change. Last section presents the experimental test carried out on one of the studied architecture.

## II. HIGH SPEED ELECTRICAL MACHINES

### A. OVERVIEW

The selection of a specific machine type, among the ones suitable for high speed operations, as suggested in literature [3] and later adopted by industry, is strongly dependent on the characteristics of the particular application [15]. Among the classical types of machines, induction (IM), switched reluctance (SR) and surface mounted permanent magnet synchronous machines (SPMSM) can all be adopted for high speed applications. The first topology can be easily employed for high speed applications, in both laminated and solid rotor variant due to the robustness of these structures [16]–[18]. In addition to that, there are no permanent magnets in the rotating part which eliminates the risk of demagnetisation. The simpler rotor construction leads to a more cost-effective solution, and does not require retaining sleeves. Drawbacks are high rotor losses, and low power factor leading to poor overall efficiency. This type of machine is thus less suitable for applications where high efficiency and power factors are crucial. SR machines are also suitable for high speed applications thanks

**TABLE 1. Machine Parameters**

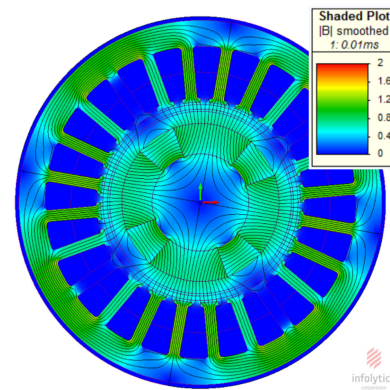
Parameter	Value	Unit
Rated power	8.5	kW
Maximum Speed	120	krpm
Stator slots	24	n.d.
Pole pairs	2	n.d.
Stator diameter	60	mm
Split ratio	0.54	p.u.
Stack length	30	mm
Airgap length	1.5	mm
Conductors per slot	14	n.d.
Strands per conductor	15	n.d.

to a simple and robust rotor design, with no active components or rotor containment system [19], [20]. The advantages of this topology are the ability to withstand harsh environments and high fault tolerance. On the other hand, efficiency and power factor both suffer the high magnetizing current; in addition at high speeds, the double salient arrangement increases the windage losses which further worsen the efficiency. The highest performance in terms of power factor, torque density and efficiency are exhibited by SPMSMs. Adopting rare-earth permanent magnets materials, with a high energy density, avoids the need for magnetizing current and increases power factor, efficiency and power density. The biggest challenge for this machine topology comes from the large forces acting on the rotor at the maximum speed. Thus, it is necessary to design and manufacture a retention system that can guarantee the integrity of the rotor [21]. Great care is required into the estimation of the additional high frequency losses the laminated iron, the magnets and retaining sleeve are subjected, so as to remain within their thermal limits of the different components of the machine [22], [23].

### B. DEVELOPED SPMSM DESIGN

Several metrics have been weighted during the design of the machine for optimum performance, and in particular power density, efficiency and power factor have been considered. The SPMSM machine has been designed with a 8.5 kW rated power, when running at 120 krpm, all the other parameters and geometrical specifications are reported in Table 1.

To achieve the best performance, an optimal distribution of losses have been derived considering a number of slot/pole and winding configurations, as shown in [24], while satisfying constraints and requirements. A distributed winding configuration with 24 slots and 4 poles has been chosen, as it meets the aforementioned goals, especially in terms of losses distribution. This allows the design of a machine where the prevailing losses are stator and rotor iron ones, reaching a compromise between efficiency and simplicity of heat extraction, leading to a easier thermal management. For the rotor design a mechanical trade-off analysis has been conducted, with the goal of determining the retaining sleeve properties such as the material and the thickness. From the rotor-dynamic point of

**FIGURE 2. Flux density distribution at no load.**

view, the first critical frequency has been designed to be at higher than the operating maximum speed. A quasi-Halbach array of samarium-cobalt magnets has been designed, with the aim of raising the fundamental flux density at the air-gap, for a higher power density, while at the same time improving manufacturability of the rotor assembly with respect to a full Halbach structure. A lamination material thickness of 0.17 mm has been chosen, in order to reduce iron losses as much as possible. Another factor that goes towards the reduction of iron losses, is the design of the machine itself, that was specifically tuned to work with low iron flux densities, as clearly shown in Fig. 2. Once the number of turns in series per phase has been chosen according to the rated voltage, the selection of the number of strands composing each conductor has been done with the aim of reducing both strand and bundle level AC copper losses [25], [26]. The cooling system was designed to limit the maximum winding temperature rise within the limit of the adopted insulation class and it is formed by a single channel water jacket surrounding the stator laminations [24] with a coolant flow rate of 15 l/m. As mentioned previously, one of the specific goals of the design was the minimization of rotor losses, i.e. eddy current losses induced in the conductive regions of the rotor by asynchronously rotating harmonic fields [27]. These harmonics are an effect generated by the interaction between slotting effect, the distortion in stator currents and the geometric distribution of conductors along the machine circumference. The chosen slot/pole combination reduces this phenomenon, when ignoring the distortion in stator currents, thus considering perfectly sinusoidal waveform. In Section IV and V the impact of current distortion introduced by the various converter architectures on the designed machine will be shown.

### III. CONVERTER ARCHITECTURES OVERVIEW

To evaluate the impact of the machine drive upon the overall system performance, three different architectures have been examined: the classic Voltage Source Inverter (VSI), that is widely used today, the Current Source Inverter (CSI), that while typically used only in very high power installations, is attractive for its potentially lower current distortion and the

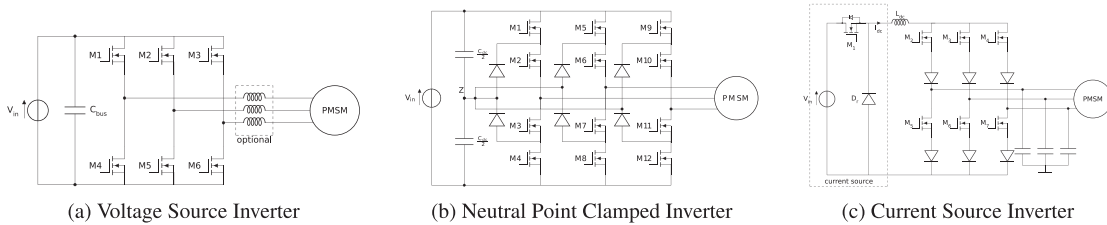


FIGURE 3. Considered converter topologies.

Neutral Point Clamped Inverter (NPC). The basic structures, shown in Fig. 3, and mode of operation of the three converters are broadly similar: a power source, appropriately filtered to form a DC-link, is fed into a full bridge type circuit that produces the desired output waveforms. The VSI uses a simple capacitor on the input, not needing any active input stages as opposed to other architectures [28] and a normal three phase bridge on the output. An output filter can be adopted in order to improve output power quality, even though it is not essential for the converter operation. The NPC is an evolution of the previous architecture, that uses three voltage levels instead of two for the output waveform synthesis. In order to accomplish this, a third level is generated by splitting the input voltage equally using two series capacitors for the DC-link. In the output section each transistor of a classic bridge is substituted with two equal switching elements in series with a diode connected between their mid-point and the mid point of the DC-link. The main advantage of this topology are the better behaviour at higher switching frequencies due to the lower voltage differences for each switching transient. The higher number of switching elements constitutes its main disadvantage, increasing the cost significantly. The last of the considered topologies is the CSI; this converter works on a dual principle with respect to the VSI. A DC current is produced by an input switching regulator, and then filtered by the large DC-Link inductance. This is then fed to the output bridge that applies it periodically to the appropriate load phase. In order to avoid voltage spikes due to the rapidly changing current on the motor inductance an output filter capacitance is necessary. The topology has various advantages, such as the possibility of a feed-forward current control and the high tolerance to overcurrent events, as the dc-link naturally limits both the maximum fault current and also its rise time. Disadvantages of this architecture include potentially slower dynamic response, when compared to voltage based converters with the same switching frequency, as the filter inductor limits the rate of change of the current, and higher power losses due to the presence of diodes in series with each switching element.

## IV. SIMULATIONS SETTINGS

### A. DRIVE SIMULATIONS

To compare the performance of the examined architectures, within the whole torque-speed plane of the machine, electro-thermal simulations have been performed in a Simulink-PLECS environment. A high value of input voltage, 600 V DC, has been considered with the aim of minimizing

the joule losses. In order to maximize the power density, minimizing both weights and volumes, no output filters have been used where possible. The high switching frequency (40 kHz) implies that the natural low pass response due to the machine inductance is strong enough not to require additional filtering. Furthermore, any additional series inductance would limit the dynamic response of the system with low impact to the output quality. The device selection has been performed on the basis of the required voltage breakdown requirement for each topology; the use of wide bandgap devices is preferred given the high operating frequencies involved. In addition to that, only monolithic devices have been considered, as series and parallel configuration, unless required by the architecture, can negatively affect the overall reliability both in terms of increased number of points of failure and uneven stress between devices as shown in [29]. For industrial application, 1200 V breakdown voltage devices constitute the most adopted solution, because of the three-phase mains can provide a DC Link voltage in the range of 600 V. Considering the technology development, 1200 V SiC devices are widely available, whereas GaN devices have been so far optimized for the low-voltage range (up to 600 V). This enables GaN devices to be used only in multi-level topologies. For this reason the gallium nitride base HEMT, with a 600 V breakdown voltage, are selected for the NPC solution, whereas the Silicon Carbide MOSFETs have been selected for the voltage and current source inverters. The choice was made to exploit the potential of the best performing technology available at the moment on the market for the different operating voltages of the devices. Another possibility is to use the same technology for all three converters, but this would disadvantage NPC unfairly. The diodes used in the CSI and NPC architectures are also based on Silicon Carbide technologies. Table 2 summarizes the main parameters that have been used for the design of each converter along with the selected devices. The power losses in the active devices can be split into conduction and switching losses [30]. The first ones are occurring when a device is conducting, they depend from the current peak magnitude  $I_m$ , its phase angle  $\theta$ , the converter modulation index  $M$  and the device on-state characteristics, in particular the on state resistance  $R_{ds}$  for MOSFETs as shown in Equation (1).

$$P_{cond} = \frac{I_m^2 R_{ds} M}{2\pi} \left( 1 + \frac{1}{3} \cos(2\theta) \right) \quad (1)$$

**TABLE 2.** Inverters Parameters

	VSI	CSI	NPC
Device brand	ST	ST + Infineon	GaN Systems
Device model	SCT20N120	SCT20N120 + IDW15S120	TPH3208P
Input filter	n.d.	1.3 $\mu$ F	n.d.
Output filter	1 $\mu$ F	5 mH	1 $\mu$ F
$f_{sw}$		40 kHz	
$V_{IN}$		600 V	

The switching losses conversely occurs only during switch transitions between conducting and blocking state. Since switching losses depends on a number of device specific parameters, which are usually not disclosed by the manufacturer, they are inferred from datasheets, which instead provide the energy loss associated with a single turn on/off event,  $E_{on}$  and  $E_{off}$ , measured in a specific operating point. In Equations (2) to (4), these values are used after normalization to calculate switching losses.

$$P_{ON} = \left( \frac{I_m V_{DC}}{\pi \cdot 2} \right) f_{sw} \frac{E_{on}}{V_{test} I_{test}} \quad (2)$$

$$P_{OFF} = \left( \frac{I_m V_{DC}}{\pi \cdot 2} \right) f_{sw} \frac{E_{off}}{V_{test} I_{test}} \quad (3)$$

$$P_{SWT} = P_{ON} + P_{OFF} \quad (4)$$

In all the performed simulations a piecewise linear approach is adopted, in order to achieve reasonable computational run time. The load currents, voltages and device losses have been saved after startup. The harmonic content of the output current has been calculated by FFT, after the application of a Hanning window, to avoid border discontinuity effects. The results from this analysis are then used to obtain a realistic losses profile of the machine, as discussed in the next sub-section.

## B. ELECTRIC MACHINE FE SIMULATIONS

The evaluation of the eddy current losses in the rotor solid components, the iron losses in the laminated one and the AC copper losses due to the non-uniform current density distribution within the slot are the main challenges related to the electromagnetic losses evaluation of high speed permanent magnet machines. While the calculation of the skin and proximity component of the AC copper losses can be carried out analytically, the determination of the circulating current requires more effort. These arise in case the single conductors are made of more parallel strands and the conductors are not transposed along the axial length of the machine. This phenomena is strictly related to the real positions of the strands inside the slot and becomes important when random wound winding are adopted as in this case study. Different works

have addressed the evaluation of circulating currents both analytically (essentially based on circuitual approach) [31] and FE study [32]. In this work, a FE simulation considering the worst case scenario in terms of conductors distribution within the slot has been carried out in order to estimate the resistance factor ( $k_{ac/dc} = R_{ac}/R_{dc}$ ) as function of the frequency. Then, the copper loss due to a certain time harmonic has been calculated from the relative dc copper loss and the resistance factor using the following formulation:

$$P_{cu} = 3R_{dc} \sum_{h=0}^{h_{max}} k_{ac/dc}(h) I(h)^2 \quad (5)$$

A modified Steinmetz model, reported in Equation (6), where  $k_h$  and  $k_e$  are respectively the hysteresis and eddy current losses coefficients fitting the manufacturer loss data, has been used to calculate the stator iron losses.

$$P_{fe} = k_h f^\alpha B^\beta + k_e (sfB)^2 \quad (6)$$

The number of steps to be used in the time-step FE simulation of the machine has been selected fixing the maximum current harmonic order to consider and the number of step needed to evaluate the latter. For all the analyzed converters and operating points, the considered maximum current harmonic order is the 100th which has been evaluated with 20 time-steps. The accurate evaluation of the eddy-current losses in the permanent magnets and the retaining sleeve require a 3D FEA with a remarkable fine mesh in the regions where the eddy current arise. Fully analytical and mixed FE-analytical methods have been proposed in the literature to avoid such high computational expensive simulation [33], [34]. In the following, the approach proposed in [35] has been adopted to calculate the eddy current losses in the solid parts of the rotor. In particular, a 2D FE simulation with an adjusted value of the permanent magnet resistivity has been carried out in order to consider its temperature variation along with a correction factor accounting for the three-dimensional nature of the problem. The following equations report the equivalent magnet resistivity  $\rho_{eq}$  as function of its temperature  $T$ , with  $a$  and  $b$  being coefficients depending on the materials, and the 3D correction factor  $F$ :

$$\rho_{eq} = \frac{bT + a}{F} \quad (7)$$

$$F = \frac{3}{4} \frac{L^2}{L^2 + w^2} \quad (8)$$

where  $L$  and  $w$  are respectively the active length and the average circumferential width of the magnets.

## V. SIMULATION RESULTS

### A. DRIVE SIMULATIONS

The losses analysis results, determined for the topologies under study, can be found in Fig. 4, for different machine operating points (33%, 66% and 100% of both rated current and maximum speed). The higher CSI losses are due to both the presence of diodes in the main current conduction path in

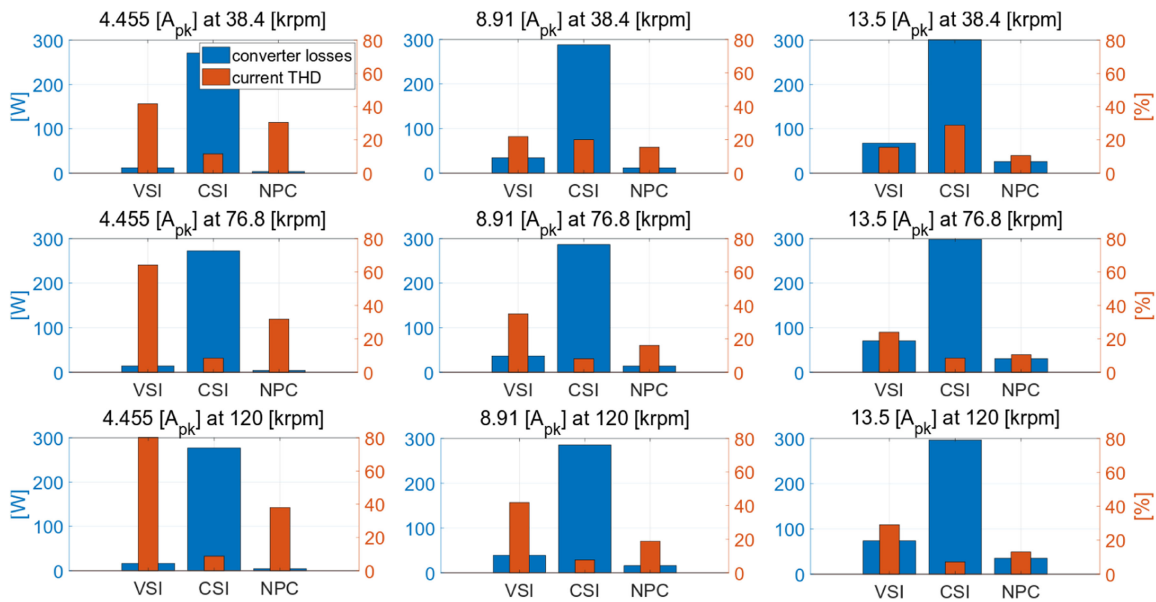


FIGURE 4. Simulated power losses and output current THD for the studied converter topologies.

addition to the switching transistors, and also to the need to keep a fixed DC-link current always circulating, for optimal dynamic performance reasons. The lowest losses have been achieved by the NPC multi-level converter, thanks to the use of a lower breakdown voltage class transistors, allowed by the lower stresses imposed to them by this architecture. The lower on state resistance of these devices not only completely offsets the higher number of conducting devices in series, but results in a net loss reduction. Clearly the losses of the three converters present an obvious strong dependence from the current rather than the frequency. With the devices choice adopted, the topology guaranteeing the lowest losses in the whole operating range is the NPC, followed by the VSI and CSI. From the analysis of current THD, also shown in Fig. 4, several remarks can be made. The CSI topology shows the lowest THD in the all operating conditions, except at lowest speed and the high currents. This is due to an undamped resonance in the LCL network constituted by DC-Link and load inductances together with the filter's capacitors. Several works are presented in literature to passively or actively damping the resonance [36], [37], but this is beyond the scope of this work. The CSI presents a very low harmonic current distortion at the maximum speed and tends to gradually worsen at lower speeds, due to the increase of the output filter gain at lower harmonics. The NPC inverter shows a lower current harmonic distortion compared to the VSI in the whole operating range. For both of them, the current THD increases as the current decreases and as the speed increases. The frequency dependence is due to the fact that low harmonics in the synthesized voltage and current, at low speed, are within the current loop bandwidth of the converter, thus partially compensated. This is a feasible approximation since a high bandwidth of the current loop is requested for high dynamic at the rated speed.

The current THD as well as its spectrum composition highly impacts the motor losses as current harmonics induce additional power losses in the electrical machine. In fact, a high harmonic content of the phase currents has a threefold effect of 1) increasing the AC copper losses, 2) creating additional asynchronously airgap magnetic fields which further increase the eddy current losses on the solid rotor parts and 3) increasing the iron losses in the stator lamination. The current waveforms obtained through the converter simulations are used to supply the electrical machine FE model and so compute the machine losses as described in the following paragraph.

## B. ELECTRICAL MACHINE SIMULATIONS

Fig. 5 shows the machine losses, whose calculation has been detailed in Section IV-B. The three main components of the machine losses, iron losses, copper losses and eddy current losses in the rotor parts, are shown considering the ideal supply condition and the current waveform provided by the three considered converters. For the ideal supply condition, the stator iron losses are the biggest contributors to global losses. During the design stage both eddy current losses in the rotor and copper losses have been minimized being these two components more difficult to extract and dissipate. As opposed to the ideal situation, when the machine is supplied with a real world converter synthesized current waveform, the distribution of the losses drastically changes. In fact, from the ideal supply condition to any of the considered converters supply, the copper losses presents the smallest increment, the iron losses increase in the range of 10–100% according to the converter and operating point, while the rotor eddy current losses exhibits the largest deviation (approximately about 10<sup>4</sup>% increment). Fig. 5(b) reports the machine losses variations respect to the ideal supply condition in logarithmic

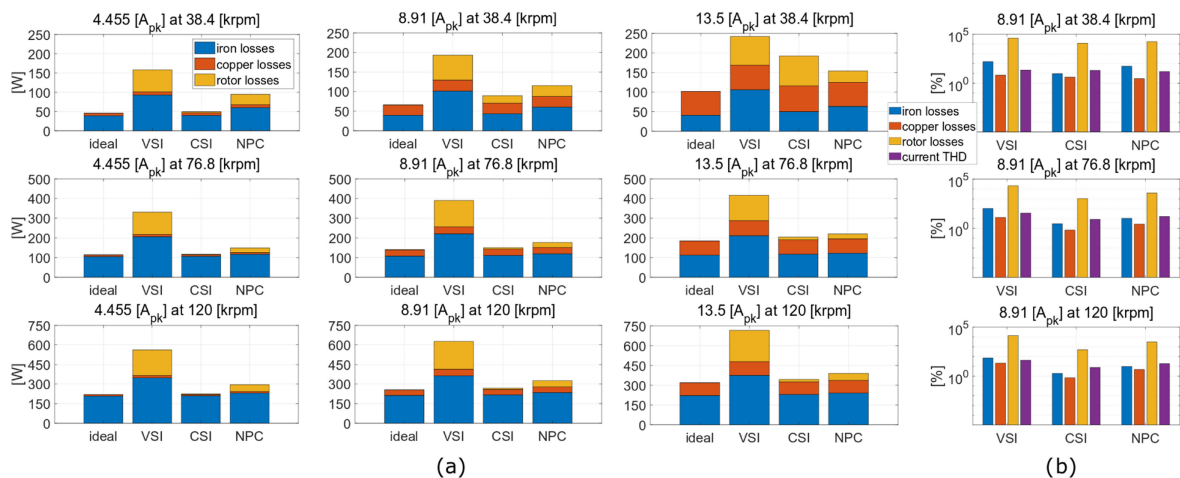


**FIGURE 5. (a) Power losses distribution of the electrical machine, (b) Power losses variations (respect to the ideal supply condition) of the electrical machine and current THD at 66% the rated current.**

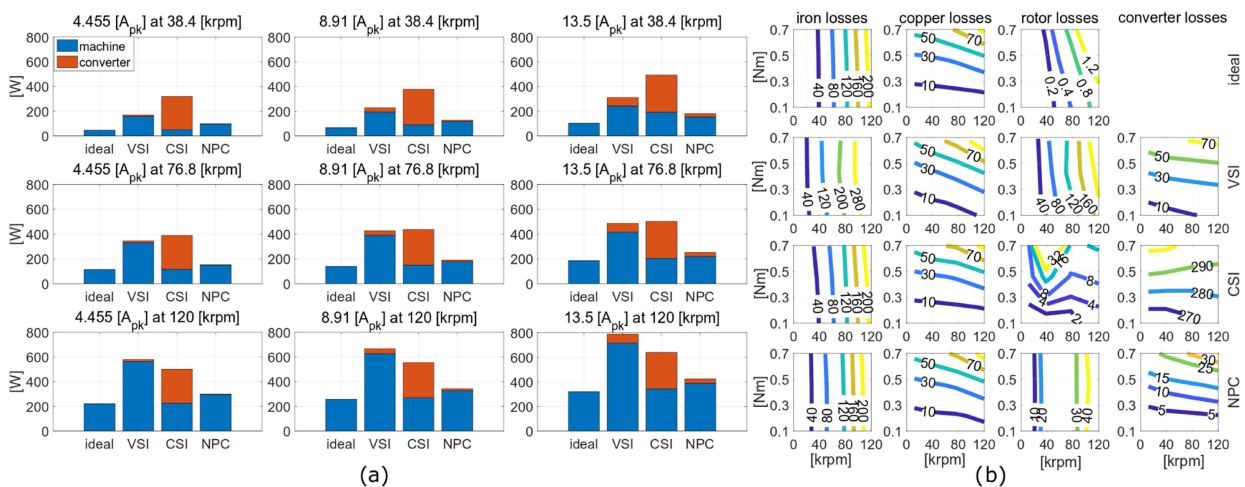


**FIGURE 6. (a) System losses distribution of the studied architectures, (b) Constant power loss loci in the torque-speed plane of all the loss component.**

scale along with the current THD only for one current level. Analysing Fig. 5 the following conclusions can be deduced.

- The least performing architecture is the VSI. It results in the the largest deviation from the ideal case in all loss components, being the stator iron losses the biggest one in absolute terms and the rotor losses in relative term.
- The best performing solution is the CSI although the NPC provides similar current THD except for low current values. This is due to the position of the current harmonics in the spectrum, the CSI provide a current waveform whose distortion is in the low frequency range leading to a lower iron and rotor losses respect to the NPC.
- All the loss increments are proportional to the current THD for any of the considered converter; when the current THDs are similar the position of the highest harmonics within the spectrum is the most influential factor affecting the machine losses (for this kind of machines it is preferable to have current harmonics of lower order).

## VI. ARCHITECTURE COMPARISON

### A. SYSTEM LOSSES AND THEIR ALLOCATION

The losses distribution of the whole system is found in Fig. 6(a). The NPC converter allows achieving the highest performance in the entire torque-speed operating plane. Comparing the CSI with the VSI, the former presents lower losses in the high-speed region while the latter performs better in the low-speed region. This behaviour can be ascribed to the different weight and rate of increment of the machine and converter losses as the speed increases. Indeed, the CSI performs better (respect to the VSI) in the high-speed region because of its low machine losses and its performance worsen as the speed decreases due to its high converter losses. The distribution of losses between the two components of the system is highly asymmetric for both VSI and NPC, i.e. the losses are mainly allocated in the electrical machine due to the high machine losses associated to the VSI and the low converter losses associated to the NPC. The CSI presents a more uniform distribution of the losses due to its high converter losses and low

**TABLE 3. Sensitivity Analysis: Input Mean and Variance for Each Considered Parameters; First Order ( $S_i$ ) and Total Order ( $S_{Ti}$ ) Sensitivity Coefficients Both for Converter Losses and Current THD**

Topology	Parameter	Input		Losses		THD	
		mean	variance	$S_i$	$S_{Ti}$	$S_i$	$S_{Ti}$
VSI	$R_{ds(ON)}$	169 m $\Omega$	10 m $\Omega$	0.194	0.115	0.041	0.324
	$f_{sw}$	40 kHz	6 kHz	0.882	0.813	0.713	1.007
CSI	$L_{DC}$	50 mH	20 mH	0.031	0.008	0.129	0.474
	$C_{FLT}$	1.3 $\mu$ F	250 nF	0.013	0.005	0.013	0.569
	$R_{ds(ON)}$	169 m $\Omega$	10 m $\Omega$	0.873	0.867	0.063	0.200
	$f_{sw}$	40 kHz	10 kHz	0.102	0.114	0.363	0.955
NPC	$R_{ds(ON)}$	75 m $\Omega$	10 m $\Omega$	0.840	0.903	0.013	0.054
	$f_{sw}$	40 kHz	10 kHz	0.209	0.202	0.945	0.940

machine losses. Fig. 6(b) shows how the losses are distributed in terms of constant loci in the torque-speed plane for the ideal as well as for the converter supply scenarios. On one hand, the NPC solution presents the lowest system losses, but it does not feature the lowest rotor losses. On the other hand, the CSI architecture exhibits high value of converter losses but it presents really low value of rotor eddy current losses. Therefore it can be stated that the NPC architecture is the best solution efficiency-wise but the CSI can allow an easier thermal management of the system being the rotor losses more difficult to extract respect to the converter losses. It is worth to underline that all the drawn considerations depend on the selected power switches technologies and the electrical machine design. Clearly in this case study, the NPC is advantaged by the adoption of 600 V GaN devices; however the consideration about the distribution of the losses remain valid also with a different devices choices.

### B. SENSITIVITY ANALYSIS

The performance of a drive depend on the value of many parameters. Since these are function of both design choices and manufacturing tolerance it is of paramount importance to correctly identify the sensitivity with respect to a variation of these quantities. The sensitivity analysis is a tool to statistically evaluate their impact on overall performance. However given the computational complexity of the analysis and the deep knowledge required to correctly identify which distribution to use for each parameter, only the following ones have been considered: switching frequency ( $f_{sw}$ ), on state resistance ( $R_{ds(ON)}$ ) of the transistors and filtering components values ( $L_{DC}$ ,  $C_{FLT}$ ). Other parameters have not been included in the analysis for a variety of reasons. Temperature for example depends too heavily on the cooling system design, which is out of the scope of this paper, to show any meaningful result; several internal device parameters could also not be included in this analysis as the range and distribution of variation is heavily dependent on the internal geometries and other manufacturing details known only to the manufacture. Various

mathematical and statistical techniques can be employed, and they can be divided into two main categories: local and global sensitivity analysis. The first class of methods rely on the analytical or numerical partial differentiation of the model, in the contour of operating points (hence local classification), with respect to the various parameters whom sensitivities needs to be evaluated. These techniques are difficult to apply because their complexity (both computational and analytical) grows rapidly as the number of variables, and repeated interactions are needed in case of multiple operating points. Global methods, by contrast, use statistical analyses in order identify the impact of a parameter variation on the model. In this study, the variance based Sobol method [38] has been adopted which is a global sensitivity analysis method. In its first step a sufficiently high number of points in the input space are randomly chosen, according to the chosen distribution of each parameter; Table 3 shows mean and standard deviations of the normal distributions used for this analyses. A simulation is then run in each one of those points. The obtained results are then used to calculate the sensitivity coefficients  $S_i$  and  $S_{Ti}$ . The former is the first order sensitivity coefficient which indicates the sensitivity of the output to first order variations of the  $i_{th}$  input parameter; the second one is the total order sensitivity coefficient that considers both first and higher order effects. The results of this analysis are always reported in Table 3. With respect to power losses, there is an interesting difference between VSI and NPC architectures. For the former, switching frequency is the most sensitive parameter, with a very high first order impact, while on state resistance is less sensitive. The NPC presents higher sensitivity to the on-state resistance value. This is due to the higher number of devices conducting the current in each converter state respect to VSI. In the CSI case, as expected, the most influential parameter is the on state resistance, the switching frequency is only marginally relevant; the impact of DC link inductance and filter capacitance value is indeed negligible. With regards to THD, the results are in line with expectations; in all the architectures, switching frequency has by far the highest impact while on





FIGURE 7. Experimental test bench.

TABLE 4. Test Rig Components

Component	Description
Drive prime mover	Control Techniques, Unidrive/SP4403
Prime mover	OSWALD, 37.5kW-20 krpm IM
Gearbox	Torquemeters Ltd, 1:5.975 ratio
Torquemeter	Torquemeters Ltd, type ET0044
Motor under test	SPM designed in house
Drive motor under test	VSI designed in house based on ROHM half bridge SiC module
Control platform drive under test	Designed in house based on Xilinx Zynq7020 SoC

state resistance has almost none. DC link inductance and filter capacitance in the CSI case have a notable impact on this figure as attested by their  $S_{Ti}$ , but this influence is only shown in the higher order index, indicating the possible interaction between these two parameters.

## VII. EXPERIMENTAL VALIDATION

With the aim of validating the reported results, a prototype of the electrical machine has been manufactured and tested using a custom VSI with SiC devices. In the following, a brief description of the experimental test bench is provided along with the results of the no-load tests and the efficiency measurements for one speed level.

### A. SETUP DESCRIPTION

The electrical machine prototype has been tested on the rig depicted in Fig. 7. The experimental test bench components have been listed in Table 4 except the auxiliary units (gearbox and torquemeters lubrication systems, cooling systems

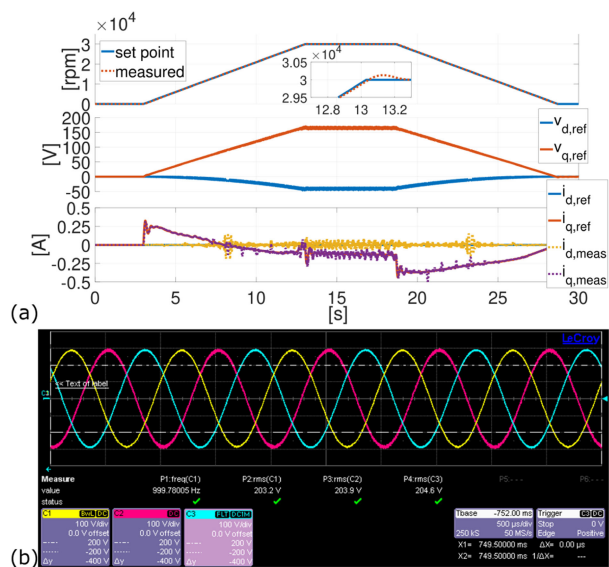


FIGURE 8. No load tests: (a) speeds, voltage and currents transient in motoring mode, (b) induced voltages in generating mode at 30 krpm.

of both prime mover and motor under test). The power converter used to supply the machine prototype is a three-phase full-bridge converter, designed in house, whose details are reported in [14]. The control algorithm was implemented on a control platform also fully designed in house whose description is detailed in [39]. During the tests, the switching frequency was set to 40 kHz as it has been considered during the power loss study.

### B. NO LOAD TEST RESULTS

Fig. 8(a) shows the transient performance acquired on the host PC from the control platform during a motoring no-load test when a trapezoidal speed reference has been imposed reaching a speed of 30 krpm. The first sub-figure shows the behaviour of the reference and measured speeds during the whole test with an inset reporting the speed signals when the steady state is reached. The other two sub-figures detail the voltage reference and the reference and measured currents in the d-q reference frame. Fig. 8(b) reports the induced voltage at 30 krpm during a generating no-load test.

### C. LOAD TEST RESULTS

Fig. 9(a) reports the measured and the estimated torque and efficiencies as function of the current load (peak value) or the mechanical power for a single operating speed (30 krpm). For each operating point the thermal steady state has been reached before measuring the input (via power analyser Newtons 4th Ltd, PPA5500) and the output power (via the torquemeter). Clearly there is a good match between the expected and the measured torque while the efficiency is underestimated in the low load range and overestimated in the high load range although the trend is respected. The highlighted discrepancy can be obviously ascribed to the accuracy of the evaluation

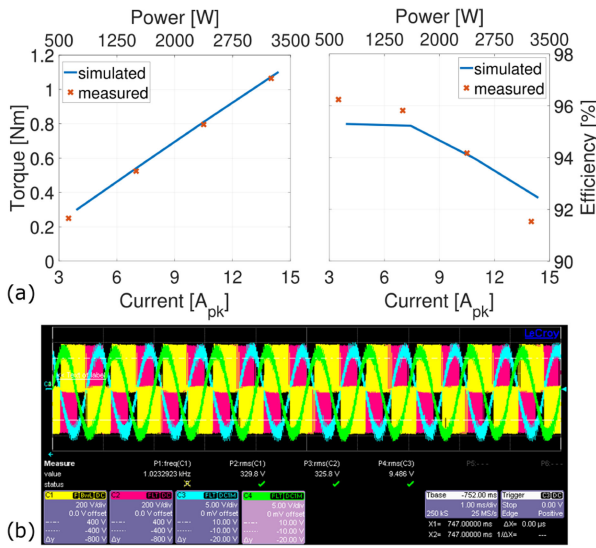


**FIGURE 9.** (a) Comparison between the measured and estimated torque and efficiency for different current levels at 30 krpm; (b) measured phase-to-phase voltages and phase currents at 30 krpm and 14  $A_{pk}$ .

methods of the different sources of the losses. Fig. 9(b) reports two phase to phase voltages and two phase currents acquired with the oscilloscope during the load test at 30 krpm and 14  $A_{pk}$ .

### VIII. CONCLUSION

This paper has presented a comparison of three drive systems having the same high speed electrical machine and three converter architectures, namely VSI, CSI and NPC. Throughout the work, the different sources of loss in the system have been deeply investigated with the aim of evaluating the impact of the converter choice on the system efficiency. To do so, first a high speed permanent magnet synchronous machine has been classically designed considering the ideal supply condition, then the drive systems featuring the three selected converters, suitably designed for the application, have been simulated in Matlab/Simulink environment. The obtained current waveforms have been then used to estimate the machine losses by FE method. The results presented in this work highlights the importance of evaluating the effect of the converter choice on the system efficiency and the need of considering how the different source of losses are distributed within the machine and between the machine and the converter. In particular, the following conclusions, summarized also in Table 5, can be drawn.

- From the converter perspective, the NPC has the lowest losses, while the CSI is the least performing in the whole operating range. This results is mainly due to the device selected for the NPC and the need of having a constant DC-link current for the CSI architecture. A different choice respectively of devices and control strategy would surely mitigate this differences but also affect the machine losses increment [28].

**TABLE 5.** Architectures Comparison; 1-Best, 3-Worst; \* Not in the Whole Operating Range

	VSI	CSI	NPC
Converter losses	2	3	1
Current THD	3	1*	2*
Machine losses	3	1	2
System losses	3*	2*	1
Rotor losses	3	1	2
Converter losses most influential parameter	$f_{sw}$	$R_{ds}$	$R_{ds}$
Current THD most influential parameter	$f_{sw}$	$f_{sw}$	$f_{sw}$
Number of devices	6	7	12

- Regarding the current THD, the CSI is the best solution although for high loads and low speeds the NPC presents similar if not slightly better values; the VSI is the worst performing choice particularly for low loads.
- The CSI topology allows achieving the lowest machine losses increment in the whole operating range except in the high-load/low-speed region. Although the NPC provides similar current THD compared to the CSI, the latter provides a current spectrum whose distortion is in the low frequency range leading to a lower iron and rotor losses respect to the NPC. The VSI architecture is the least performing one. These considerations are deeply affected by the machine design, in particular the distribution between iron, copper and rotor losses. In fact a different distribution of the losses (i.e. less iron more copper losses) would have disadvantaged less the VSI respect to the other two architectures.
- System-wise, the NPC provides the highest efficiency for all the operating points. The CSI performs better than the VSI in the high-speed region because of its low machine losses and its performance worsen as the speed decreases due to its high converter losses.
- Although the NPC is best from the drive efficiency point of view, it is not the solution providing the lowest machine rotor losses. The latter are definitely more difficult to extract respect to the iron and copper losses of the machine and the converter losses. From this standpoint, the CSI architecture presents the lowest rotor eddy current losses at the expense of higher converter losses.
- The NPC and CSI converter losses are highly affected by the variation of the on-state resistance while the VSI one is more sensible to the switching frequency change.
- The current THD and so the machine losses are definitely more sensible to the variation of the switching frequency.
- In spite of the better system efficiency, the NPC also shows a greater hardware and software complexities respect to the other two architectures. This is mainly due to the higher number of devices, that require more articulated gate driver circuit and PWM strategies to balance the neutral point voltage.

The loss trend has been validated experimentally for the VSI architecture, showing a good agreement between the expected and the measured efficiency.

## REFERENCES

- [1] G. Buticchi, S. Bozhko, M. Liserre, P. Wheeler, and K. Al-Haddad, "On-board microgrids for the more electric aircraft—Technology review," *IEEE Trans. Ind. Electron.*, vol. 66, no. 7, pp. 5588–5599, Jul. 2019.
- [2] W. Cao, B. C. Mecrow, G. J. Atkinson, J. W. Bennett, and D. J. Atkinson, "Overview of electric motor technologies used for more electric aircraft (MAE)," *IEEE Trans. Ind. Electron.*, vol. 59, no. 9, pp. 3523–3531, Sep. 2012.
- [3] R. Abebe, M. D. Nardo, D. Gerada, G. L. Calzo, L. Papini, and C. Gerada, "High speed drives review: Machines, converters and applications," in *Proc. IECON 42nd Annu. Conf. IEEE Ind. Electron. Soc.*, Oct. 2016, pp. 1675–1679.
- [4] D. Gerada, A. Mebarki, N. L. Brown, C. Gerada, A. Cavagnino, and A. Boglietti, "High-speed electrical machines: Technologies, trends, and developments," *IEEE Trans. Ind. Electron.*, vol. 61, no. 6, pp. 2946–2959, Jun. 2014.
- [5] W. Lee, E. Schubert, Y. Li, S. Li, D. Bobba, and B. Sarlioglu, "Overview of electric turbocharger and supercharger for downsized internal combustion engines," *IEEE Trans. Transp. Electrific.*, vol. 3, no. 1, pp. 36–47, Mar. 2017.
- [6] D. Lusignani, D. Barater, G. Franceschini, G. Buticchi, M. Galea, and C. Gerada, "A high-speed electric drive for the more electric engine," in *Proc. IEEE Energy Convers. Congr. Expo.*, Sep. 2015, pp. 4004–4011.
- [7] S. Li, Y. Li, W. Choi, and B. Sarlioglu, "High-speed electric machines: Challenges and design considerations," *IEEE Trans. Transp. Electrific.*, vol. 2, no. 1, pp. 2–13, Mar. 2016.
- [8] B. Zhang and S. Wang, "A survey of EMI research in power electronics systems with wide bandgap semiconductor devices," *IEEE J. Emerg. Sel. Topics Power Electron.*, vol. 8, no. 1, pp. 626–643, Mar. 2020.
- [9] L. Concari, D. Barater, G. Buticchi, C. Concari, and M. Liserre, "H8 inverter for common-mode voltage reduction in electric drives," *IEEE Trans. Industry Appl.*, vol. 52, no. 5, pp. 4010–4019, Sep./Oct. 2016.
- [10] D. R. Meyer, A. Cavallini, L. Lusuardi, D. Barater, G. Pietrini, and A. Soldati, "Influence of impulse voltage repetition frequency on RPDIV in partial vacuum," *IEEE Trans. Dielectr. Elect. Insul.*, vol. 25, no. 3, pp. 873–882, Jun. 2018.
- [11] L. Clotea and A. Forcos, "Power losses evaluation of two and three-level NPC inverters considering drive applications," in *Proc. 13th Int. Conf. Optim. Elect. Electron. Equip.*, May 2012, pp. 929–934.
- [12] R. Andersson and A. Reinap, "Loss mapping of an insert permanent magnets synchronous machine for parallel hybrid electric heavy vehicles," in *Proc. 22nd Int. Conf. Elect. Mach.*, Sep. 2016, pp. 1847–1853.
- [13] L. Schwager, A. Tüysüz, C. Zwyssig, and J. W. Kolar, "Modeling and comparison of machine and converter losses for PWM and PAM in high-speed drives," *IEEE Trans. Ind. Appl.*, vol. 50, no. 2, pp. 995–1006, Mar. 2014.
- [14] G. L. Calzo, P. Zanchetta, C. Gerada, A. Gaeta, and F. Crescimbin, "Converter topologies comparison for more electric aircrafts high speed starter/generator application," in *Proc. IEEE Energy Convers. Congr. Expo.*, Sep. 2015, pp. 3659–3666.
- [15] J. B. Bartolo, H. Zhang, D. Gerada, L. D. Lillo, and C. Gerada, "High speed electrical generators, application, materials and design," in *Proc. IEEE Workshop Elect. Mach. Des., Control Diagnosis*, Mar. 2013, pp. 47–59.
- [16] J. Pyrhonen, J. Nerg, P. Kurronen, and U. Lauber, "High-speed high-output solid-rotor induction-motor technology for gas compression," *IEEE Trans. Ind. Electron.*, vol. 57, no. 1, pp. 272–280, Jan. 2010.
- [17] J. F. Gieras and J. Saari, "Performance calculation for a high-speed solid-rotor induction motor," *IEEE Trans. Ind. Electron.*, vol. 59, no. 6, pp. 2689–2700, Jun. 2012.
- [18] D. Gerada, A. Mebarki, N. L. Brown, K. J. Bradley, and C. Gerada, "Design aspects of high-speed high-power-density laminated-rotor induction machines," *IEEE Trans. Ind. Electron.*, vol. 58, no. 9, pp. 4039–4047, Sep. 2011.
- [19] J. Borg Bartolo, M. Degano, J. Espina, and C. Gerada, "Design and initial testing of a high-speed 45-kW switched reluctance drive for aerospace application," *IEEE Trans. Ind. Electron.*, vol. 64, no. 2, pp. 988–997, Feb. 2017.
- [20] M. D. Nardo, G. L. Calzo, M. Galea, and C. Gerada, "Design optimization of a high-speed synchronous reluctance machine," *IEEE Trans. Ind. Appl.*, vol. 54, no. 1, pp. 233–243, Jan./Feb. 2018.
- [21] A. Binder, T. Schneider, and M. Klohr, "Fixation of buried and surface-mounted magnets in high-speed permanent-magnet synchronous machines," *IEEE Trans. Ind. Appl.*, vol. 42, no. 4, pp. 1031–1037, Jul./Aug. 2006.
- [22] S. Jumayev, M. Merdzan, K. O. Boynov, J. J. H. Paulides, J. Pyrhönen, and E. A. Lomonova, "The effect of PWM on rotor eddy-current losses in high-speed permanent magnet machines," *IEEE Trans. Magn.*, vol. 51, no. 11, Nov. 2015, Art. no. 8109204.
- [23] Z. Zhu et al., "Evaluation of iron loss models in electrical machines," *IEEE Trans. Ind. Appl.*, vol. 55, no. 2, pp. 1461–1472, Mar./Apr. 2019.
- [24] D. Borg-Bartolo, D. Gerada, C. Micallef, A. Mebarki, N. L. Brown, and C. Gerada, "Thermal modelling and selection of a high speed permanent magnet surface mount electrical machine," in *Proc. 6th IET Int. Conf. Power Electron., Mach. Drives*, Mar. 2012, pp. 1–6.
- [25] P. B. Reddy and T. M. Jahns, "Analysis of bundle losses in high speed machines," in *Proc. Int. Power Electron. Conf.*, Jun. 2010, pp. 2181–2188.
- [26] A. Fatemi, D. M. Ionel, N. A. O. Demerdash, D. A. Staton, R. Wrobel, and Y. C. Chong, "Computationally efficient strand eddy current loss calculation in electric machines," *IEEE Trans. Ind. Appl.*, vol. 55, no. 4, pp. 3479–3489, Jul./Aug. 2019.
- [27] F. Luise, A. Tassarolo, F. Agnolet, and M. Mezzarobba, "Use of time-harmonic fe analysis to compute rotor eddy-current losses in synchronous machines subject to distorted stator currents," in *Proc. 20th Int. Conf. Elect. Mach.*, Sep. 2012, pp. 1503–1509.
- [28] F. Savi, D. Barater, M. D. Nardo, M. Degano, and C. Gerada, "A system level comparison of drive topologies for high speed electrical machines," in *Proc. 43rd Annu. Conf. IEEE Ind. Electron. Soc.*, Oct. 2017, pp. 4357–4362.
- [29] J. Hu et al., "Robustness and balancing of parallel-connected power devices: SiC Versus CoolMOS," *IEEE Trans. Ind. Electron.*, vol. 63, no. 4, pp. 2092–2102, Apr. 2016.
- [30] A. Wintrich, U. Nicolai, W. Tursky, and T. Reimann, *Application Manual Power Semiconductors*. SEMIKRON International GmbH, 2015.
- [31] A. Lehikoinen, N. Chiodetto, E. Lantto, A. Arkkio, and A. Belahcen, "Monte Carlo analysis of circulating currents in random-wound electrical machines," *IEEE Trans. Magn.*, vol. 52, no. 8, pp. 1–12, Aug. 2016.
- [32] M. van der Geest, H. Polinder, J. A. Ferreira, and D. Zeilstra, "Current sharing analysis of parallel strands in low-voltage high-speed machines," *IEEE Trans. Ind. Electron.*, vol. 61, pp. 3064–3070, Jun. 2014.
- [33] A. Tassarolo, "A survey of state-of-the-art methods to compute rotor eddy-current losses in synchronous permanent magnet machines," in *Proc. IEEE Workshop Elect. Mach. Design, Control Diagnosis*, Apr. 2017, pp. 12–19.
- [34] X. Wu, R. Wrobel, P. H. Mellor, and C. Zhang, "A computationally efficient pm power loss mapping for brushless AC PM machines with surface-mounted PM rotor construction," *IEEE Trans. Ind. Electron.*, vol. 62, no. 12, pp. 7391–7401, Dec. 2015.
- [35] S. Ruoho, T. S. Nokki, J. Kolehmainen, and A. Arkkio, "Modeling magnet length in 2-D finite-element analysis of electric machines," *IEEE Trans. Magn.*, vol. 45, no. 8, pp. 3114–3120, Aug. 2009.
- [36] M. Mao, S. Weng, F. Liu, L. Chang, M. Ding, and H. Wu, "A novel PRD control method damping resonance in grid-connected three-phase SVPWM current source inverter," in *Proc. 3rd IEEE Int. Symp. Power Electron. Distrib. Gener. Syst.*, Jun. 2012, pp. 487–491.
- [37] I. Chtouki, M. Zazi, M. Feddi, and M. Rayyam, "LCL filter with passive damping for PV system connected to the network," in *Proc. Int. Renewable Sustain. Energy Conf.*, Nov. 2016, pp. 692–697.
- [38] M. J. Jansen, "Analysis of variance designs for model output," *Comput. Phys. Commun.*, vol. 117, no. 1, pp. 35–43, 1999.
- [39] A. Galassini, G. Lo Calzo, A. Formentini, C. Gerada, P. Zanchetta, and A. Costabeber, "Ucube: Control platform for power electronics," in *Proc. IEEE Workshop Elect. Mach. Des., Control Diagnosis*, Apr. 2017, pp. 216–221.



**FILIPPO SAVI** (Student Member, IEEE) received the master's degree in electronic engineering from the University of Parma, Parma, Italy, in 2017, he is currently working toward the Ph.D. degree with the University of Nottingham, Nottingham, U.K. His research interests include high speed drives, modular and fault tolerant power electronics for transportation electrification. Digital communications for high performance, low latency and jitter for high bandwidth feedback control.



**DAVIDE BARATER** (Member, IEEE) received the master's degree in electronic engineering and the Ph.D. degree in information technology from the University of Parma, Parma, Italy, 2009 and 2014, respectively. He was an Honorary Scholar with the University of Nottingham, U.K., during 2012, and a Visiting Researcher with the University of Kiel, Kiel, Germany, in 2015. He is currently an Assistant Professor with the Department of Engineering "Enzo Ferrari," University of Modena and Reggio Emilia, Modena, Italy. He is the author or coauthor

of more than 60 international papers. His research area is focused on power electronics for e-mobility and motor drives. He is the Coordinator of two European Project: RAISE, to evaluate the impact of the high voltage gradients, introduced by the fast commutations of new wide bandgap power devices (SiC, GaN), on the life time of electrical motor insulation systems. AUTO-MEA that aims to develop electrical motors and drives for next generation of electrical mobility. In particular, novel solutions for windings structures and cooling systems for improved power density, efficiency and increased frequency operation. He is an Associate Editor for the IEEE TRANSACTIONS ON INDUSTRY APPLICATIONS



**MAURO DI NARDO** (Member, IEEE) received the M.Sc. (Hons.) degree in electrical engineering from the Polytechnical University of Bari, Bari, Italy, in 2012, and the Ph.D. degree in electrical machine design from the University of Nottingham, Nottingham, U.K., in 2017. From 2017 to 2019 he was the Head of the AROL research team within the Polytechnical University of Bari leading industrial R&D projects on electrical drives design for mechatronics applications. Since the 2019, he has been joined the Power Electronics and Machine

Control Group, University of Nottingham as Research Fellow. His research interests are the analysis, modeling, and optimizations of electrical machines, including permanent magnet and synchronous reluctance topologies for automotive and aerospace sectors as well as induction motor for industrial applications.



**MICHELE DEGANO** (Member, IEEE) received the Laurea degree in electrical engineering from the University of Trieste, Trieste, Italy, in 2011, and the Ph.D. degree in industrial engineering from the University of Padova, Padova, Italy in 2015. In 2015, he joined the Power Electronics, Machines and Control Group, The University of Nottingham, Nottingham, U.K., as a Research Fellow, where he is currently an Assistant Professor teaching advanced courses on electrical machines. His main research interests include design and optimization

of permanent-magnet machines, reluctance and permanent-magnet-assisted synchronous reluctance motors through genetic optimization techniques, for automotive and aerospace applications.



**PAT WHEELER** (Senior Member, IEEE) received the B.Eng. (Hons.) degree from the University of Bristol, Bristol, U.K. He received the Ph.D. degree in electrical Engineering for his work on Matrix Converters from the University of Bristol, U.K. in 1994. In 1993, he moved to the University of Nottingham and worked as a Research Assistant with the Department of Electrical and Electronic Engineering. In 1996, he became a Lecturer in the Power Electronics, Machines and Control Group with the University of Nottingham, U.K. Since January

2008, he has been a Full Professor in the same research group. He was the Head of the Department of Electrical and Electronic Engineering, University of Nottingham from 2015 to 2018. He is currently the Head of the Power Electronics, Machines and Control Research Group and is the Li Dak Sum Chair Professor in Electrical and Aerospace Engineering with the University of Nottingham, China. He has authored 500 academic publications in leading international conferences and journals. He is a member of the IEEE PELs AdCom and was an IEEE PELs Distinguished Lecturer from 2013 to 2017.



**CHRIS GERADA** (Senior Member, IEEE) received the Ph.D. degree in numerical modeling of electrical machines from the University of Nottingham, Nottingham, U.K., in 2005. He subsequently worked as a Researcher with the University of Nottingham on high-performance electrical drives and on the design and modeling of electromagnetic actuators for aerospace applications. He was appointed a Lecturer in electrical machines in 2008, an Associate Professor in 2011, and a Professor in 2013. He has secured major industrial, European

and UK grants, authored more than 200 papers and has been awarded a Royal Academy of Engineering Research Chair to consolidate research in the field. His core research interests include the design and modeling of high-performance electric drives and machines. He is an Associate Editor for the IEEE TRANSACTION ON INDUSTRY APPLICATIONS.



**GIAMPAOLO BUTICCHI** (Senior Member, IEEE) received the master's degree in electronic engineering and the Ph.D. degree in information technologies from the University of Parma, Parma, Italy, in 2009 and 2013. In 2012, he was Visiting Researcher with The University of Nottingham, Nottingham, U.K. Between 2014 and 2017, he was a Postdoctoral Researcher and Von Humboldt Postdoctoral Fellow with the University of Kiel, Kiel, Germany.

He is currently an Associate Professor in electrical engineering with The University of Nottingham, Ningbo, China and the Head of Power Electronics of the Nottingham Electrification Center. He is author/co-author of more than 200 scientific papers. His research focuses on power electronics for renewable energy systems, smart transformer fed micro-grids and dc grids for the More Electric Aircraft. He is an Associate Editor for the IEEE TRANSACTIONS ON INDUSTRIAL ELECTRONICS and of the IEEE TRANSACTIONS ON TRANSPORTATION ELECTRIFICATION.

He is the Chair of the IEEE Industrial Electronics Society Technical Committee on Renewable Energy Systems.